Journal of Materials Chemistry A

PAPER

View Article Online
View Journal | View Issue

Cite this: J. Mater. Chem. A, 2015, 3, 4738

MIL-101(Fe) as a lithium-ion battery electrode material: a relaxation and intercalation mechanism during lithium insertion†

JaeWook Shin,[a] Min Kim,‡[b] Jordi Cirera,[b] Shawn Chen,[a] Gregory J. Halder,[c] Thomas A. Yersak,[a] Francesco Paesani,[b] Seth M. Cohen[b] and Ying Shirley Meng*[a]

Received 6th December 2014
Accepted 14th January 2015

DOI: 10.1039/c4ta06694d

www.rsc.org/MaterialsA

The electrochemical performance of a MIL-101(Fe) metal–organic framework (MOF) as a lithium ion battery electrode is reported for the first time. Iron metal centers can be electrochemically activated. The Fe^{3+}/Fe^{2+} redox couple is electrochemically active, but not reversible over many cycles. A comparison between *ex situ* and *in operando* X-ray absorption spectroscopy (XAS) on the Fe K-edge is presented. Our results indicate that the capacity fade is related to a time dependent, irreversible oxidation of Fe^{2+} to Fe^{3+}. These results are key in proving the importance of *in operando* XAS measurements. The MOF side reaction with an electrolyte has been computationally modeled. These results provide further insights on the mechanism responsible for the MOF lack of reversibility. Future guidelines for improving the reversibility of MOFs used as electrodes in Li-ion batteries based on the fine-tuning of the electronic structure of the material are proposed.

Introduction

Rechargeable Li-ion batteries are essential for the development of smartphones, laptop computers, and many other technologies including grid energy storage.[1] The materials used in commercial Li-ion batteries are far too expensive and energy intensive for large-scale grid storage applications.[1–4] For example, layered oxide cathode materials are costly because they require a high temperature synthesis process and contain expensive transition metals like Co.[5–8] In order to reduce the cost of Li-ion batteries for grid scale applications, metal–organic framework (MOF) cathode materials could be utilized. MOF materials offer several advantages with respect to other porous materials because of their flexible synthetic routes, low temperature synthesis, and comparatively inexpensive precursor materials.[9]

MOFs represent a relatively new class of porous materials assembled from two main components: an inorganic secondary building unit (SBU) and an organic linker.[10] The SBUs are generally composed of transition metal ions or small metal clusters, while the organic linkers include a wide range of molecules, such as dicarboxylates, with 1,4-benzene dicarboxylic acid (H_2bdc) being among the most commonly utilized ligands.[11] The Zn_4O(4,4′,4″-benzene-1,3,5-triyl-tri-benzoate)$_2$ (MOF-177) was the first MOF to be studied as a host for lithium insertion.[12] Unfortunately, MOF-177 does not exhibit good electrochemical reversibility. Shortly after this initial study, two Fe^{3+}-based MOFs – $Fe(OH)_{0.8}F_{0.2}$(bdc) (MIL-53(Fe)) and FeOH(bdc) (MIL-68(Fe), MIL = Materials of Institut Lavoisier) – were synthesized and tested as battery materials.[13,14] MIL-53(Fe) exhibits good electrochemical reversibility and was found to be superior to MIL-68(Fe).[14,15] However, the synthesis of MIL-53(Fe) requires HF, which limits its potential as a large scale grid storage battery material. To avoid the use of HF, MIL-101(Fe) was chosen as an electrode candidate. The MIL-101(Fe) SBU is composed of a carboxylate-bridged, oxo-centered, trinuclear Fe^{3+} complex (Fig. 1a). This particular SBU complex is a well-known motif in inorganic chemistry, and its electron density distribution, magnetic, and electrochemical properties have been previously reported.[15–17] The theoretical capacity of the material with one lithium insertion per Fe atom is 107.74 mA h g^{-1}.

Using powder X-ray diffraction (PXRD) and X-ray absorption spectroscopy (XAS), we find that MIL-101(Fe) undergoes structurally reversible intercalation reactions, with the Fe^{3+}/Fe^{2+} redox couple being electrochemically active. However, in long term cycling, we observe an exponential decay in reversible lithium insertion capacity. To evaluate the irreversibility associated with MIL-101(Fe), *ex situ* and *in operando* XAS

[a]Department of Nanoengineering, University of California, San Diego, La Jolla, California 92093, USA. E-mail: shmeng@ucsd.edu; Fax: +1 8585349553; Tel: +1 8588224247

[b]Department of Chemistry and Biochemistry, University of California, San Diego, La Jolla, California 92093, USA

[c]X-ray Science Division, Advanced Photon Source, Argonne National Laboratory, Argonne, Illinois 60439, USA

† Electronic supplementary information (ESI) available. See DOI: 10.1039/c4ta06694d

‡ Present address: Department of Chemistry, Chungbuk National University, 1 Chungdae-ro, Seowon-gu, Cheongju-si, 362-763, Republic of Korea.

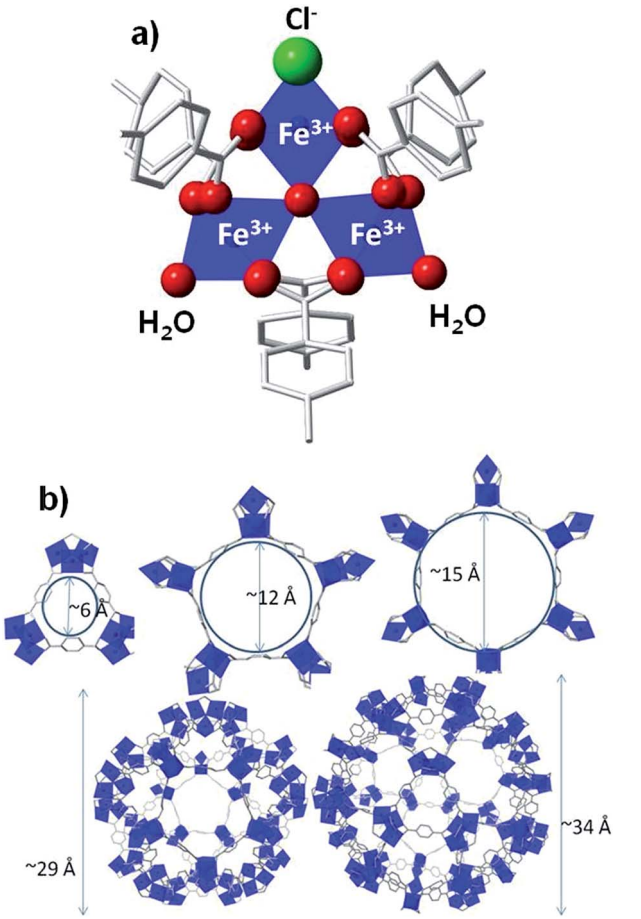

Fig. 1 Structure of MIL-101(Fe). (a) The SBU (blue, Fe; red, O; stick, C; green, Cl; H is omitted for clarity). (b) The windows and pores of MIL-101(Fe) with Cl and O atoms omitted for clarity.

experiments are conducted. The two types of XAS results reveal Fe^{2+} relaxation back to the pristine Fe^{3+}. To rationalize this phenomenon, electronic structure calculations were conducted to model the side reactions responsible for the lack of reversibility. We propose that the observed Fe^{2+} to Fe^{3+} relaxation promotes irreversible accumulation of lithium in MIL-101(Fe), which leads to the poor capacity retention.

Experimental and computational methods

MIL-101(Fe) preparation

MIL-101(Fe) was prepared by using a modified procedure.[18] Equimolar (0.346 mmol) $FeCl_3 \cdot 5H_2O$ (Sigma Aldrich) and H_2bdc (Sigma Aldrich) were dissolved in 15 mL *N*,*N*-dimethyl formamide (DMF, Alfa Aesar). This solution was then heated to 150 °C for 15 min *via* microwave irradiation (CEM discover S-class microwave reactor). After cooling to room temperature, the particles were filtered and washed with 20 mL of DMF and methanol.[18] After washing, the product was dried to evacuate water molecules trapped in the pores. Water can deteriorate the quality of the battery electrolyte. Drying was performed at 150 °C under vacuum for 3 h. After the drying process, the product was transferred into a dry glove box (MBraun) filled with high purity Argon (Ar) without exposure to air (Fig. S1†).

Electrochemical testing

Unless otherwise noted, electrochemical cells were constructed using Swagelok cells with 0.5 inches diameter stainless steel rods as the current collector. Following a previously outlined procedure,[19] assembly was conducted in an Ar filled glove box with Li metal foil (Sigma Aldrich) used as the counter electrode, Whatman GF/D borosilicate glass fiber sheets used as the separators, and 1 M $LiPF_6$ in 1 : 1 (by weight) ethylene carbonate : dimethyl carbonate (EC : DMC) (BASF, 1.6 PPM of water) used as the electrolyte. The working electrodes were prepared by ball milling (Retsch PM 100) carbon black (Super-P (SP), Timcal) and MIL-101(Fe) powders in a weight ratio of 3 : 7, respectively. Specifically, 100 mg total of the powder was milled at 100 rpm for 10 min in a 50 mL agate (Retsch Part # 01.462.0139) jar with a ball to powder weight ratio of 120 : 1, respectively. Cells were cycled under galvanostatic conditions at room temperature using an Arbin BT 2100 battery tester between the voltages of 2.0 and 3.5 V (*versus* Li^+/Li) at rates of C/60, C/40, C/20, and C/10. Theoretical capacity was calculated assuming the complete one electron redox reaction of the Fe^{3+}/Fe^{2+} redox couple.

Powder X-ray diffraction

The cycled MIL-101(Fe) material used in the PXRD was prepared at a rate of C/40. After cycling was complete, the electrode was recovered from the disassembled Swagelok cell and washed with dimethyl carbonate (DMC). Upon drying in an Ar environment, the sample was placed inside a kapton capillary tube and sealed with epoxy glue. *Ex situ* synchrotron powder diffraction experiments were performed using the monochromated X-rays (0.6661 Å, 300 μm diameter beam size) available at the 1-BM beamline of the Advanced Photon Source (Argonne National Laboratory). The samples were sealed in 0.9 mm diameter polyimide capillaries. Diffraction data were collected using a Perkin-Elmer flat panel area detector (XRD 1621 CN3-EHS) over the *d*-spacing range 1–50 Å. The raw images were processed within Fit-2D,[20,21] refining the sample-to-detector distance and tilt of the detector relative to the beam based on the data obtained for a LaB_6 standard.

X-ray absorption spectroscopy

In operando XAS was performed at the Stanford Synchrotron Radiation Lightsource (SSRL) using the fluorescence mode of beamline 4-1. The *in operando* battery was assembled using a custom designed coin cell with a Cirlex film (Fralock) as the X-ray transparent window and cycled at a rate of C/20 during *in operando* XAS measurements. Transmission mode *ex situ* XAS experiments were performed at APS 9-BM. Electrode samples were prepared as outlined above for the PXRD samples. After drying, the sample was sealed between two layers of Kapton tape (http://KaptonTape.com). For both experiments, the XANES (X-ray Absorption Near Edge Spectroscopy) region normalization and

the EXAFS (Extended X-ray Absorption Fine Structure) region Fourier transformation were done using Athena software.[22] The extracted EXAFS signals $\chi(k)$, were weighted by k^2 to emphasize the high-energy oscillations and the signals were then Fourier-transformed in a k-range of 2.0–10.0 Å^{-1} (*in operando*) or 2.0–9.0 Å^{-1} (*ex situ*). During the Fourier-transform, a Hanning termination window with a dk value of 1 was utilized to obtain the magnitude plots of the EXAFS spectra in an R-space (Å).

Computational methods

All calculations were performed with Gaussian 09 (Rev C.01) using the hybrid B3LYP functional with a 10^{-8} convergence criterion for the elements of the density matrix.[23] The fully optimized contracted triple-ζ all-electron Gaussian basis set developed by Ahlrichs and co-workers was employed for all atoms, with the addition of polarization functions for Fe.[24] Vibrational analysis was performed for all the optimized structures, and the corresponding harmonic frequencies were used to estimate the thermodynamic quantities. The MIL-101(Fe) secondary building unit was properly modeled for computational efficiency (Fig. S2†). The different spin topologies were modeled using the fragments option, which allows the definition of specific electronic structures for each metal center. The broken-symmetry solutions were spin-projected by using eqn (1), were J is the exchange coupling constant, E_{BS} is the energy of the broken symmetry state, E_{HS} is the energy of the highest spin state, $\langle S^2\rangle_{BS}$ is the spin expected value of the total spin for the broken symmetry, and $\langle S^2\rangle_{HS}$ is the spin expected value of the total spin for the highest spin state,

$$J = \frac{2(E_{BS} - E_{HS})}{\langle S^2\rangle_{HS} - \langle S^2\rangle_{BS}} \quad (1)$$

Results

Fig. 2 presents the electrochemical performance of MIL-101(Fe) electrodes *versus* Li counter electrodes. Upon initial lithiation (Fig. 2a), it was found that MIL-101(Fe) accommodates 0.62 Li/Fe. Compared to previous reports, this value is similar to that of MIL-53(Fe) (~0.62 Li/Fe) and higher than that of MIL-68(Fe) (~0.35 Li/Fe). However, MIL-101(Fe) achieves this value at a higher voltage cutoff of 2.0 V (1.5 V cutoff for MIL-53(Fe) and MIL-68(Fe)). The initial Coulombic efficiency for MIL-101(Fe) is 79%, which is lower than the value previously reported for MIL-53(Fe) (~97%) but close to that measured for MIL-68(Fe) (~79%). Due to this irreversibility, MIL-101(Fe) exhibits poor capacity retention and accommodates only 0.37 Li/Fe by the 5th cycle.

To characterize the electrochemistry of MIL-101(Fe), we studied the differential capacity (dQ/dV) of the first 5 cycles (Fig. 2b). During the first cycle, we observed five distinct reduction peaks at 2.99, 2.59, 2.42, 2.27, and 2.13 V as well as two distinct oxidation peaks at 2.87 and 3.00 V. Multiple peaks are expected because MIL-101(Fe) has a complex SBU structure with several different Li insertion sites. A previous computational study found that MIL-53(Fe) has at least two distinct sites available for Li insertion.[25] A set of *ex situ* XAS data suggests that at least two different reactions occurred upon lithiation of MIL-101(Fe) (Fig. S3 and S4†). Exact assignment of redox peaks to particular lithiation sites is best left to computational studies

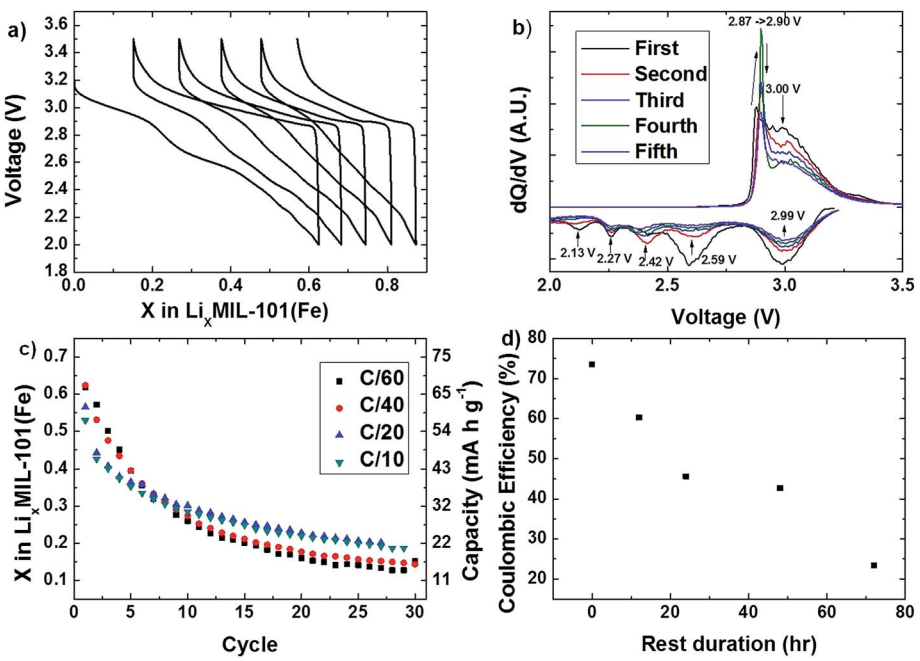

Fig. 2 Results of galvanostatically cycling MIL-101(Fe) electrodes *versus* a Li counter electrode. (a) First five voltage profiles at a rate of C/40. (b) Differential capacity (dQ/dV) of the first 5 cycles at a rate of C/40. (c) Cyclic capacity of MIL-101(Fe) electrodes at a variety of different C-rates. (d) First cycle Coulombic efficiency of MIL-101(Fe) electrodes which were rested between discharge (C/20) and charge (C/20) for different amounts of time. Coulombic efficiency decreases as the rest time is increased.

beyond the scope of this work. In the subsequent cycles, the 2.42 V reduction peak and the 2.87 V oxidation peak increased in intensity while all other peaks reduced in intensity. With extended cycling, it was observed that all oxidation and reduction peaks decreased in intensity (Fig. S5†). It is noted that the 2.99 V and 2.59 V reductive peaks fade at much different rates. A different rate of degradation indicates that the observed irreversibility of MIL-101(Fe) may be associated with a particular Li insertion site.

In order to study how the rate of lithiation/de-lithiation affects reversibility, MIL-101(Fe) cells were cycled for 30 cycles at rates of C/60, C/40, C/20, and C/10 (Fig. 2c). Initially, faster rates were associated with lower degrees of lithiation; however, with extended cycling the cells cycled at faster rates exhibited better capacity retention than the cells cycled at slower rates. Specifically, the C/60 cell delivered a 30^{th} cycle discharge capacity of only 0.1 Li/Fe while the C/10 cell delivered a 30^{th} cycle discharge of 0.2 Li/Fe. The C/10 cell delivered a higher 30^{th} cycle discharge capacity in spite of accommodating the least amount of lithium on the first cycle. This result clearly indicated that there is a stability issue with the lithiated state of the MOF.

To further investigate the dependency that the rate has upon capacity retention, we studied how incorporating an open-circuit voltage rest into the cycling protocol affects the reversibility of lithium extraction. After being discharged at a rate of C/20, the MIL-101(Fe) cells were rested for 0, 10, 20, 50, or 72 hours and then charged at a rate of C/20. Fig. 2d shows that the percentage of lithium extracted was dependent upon the duration of the rest step. If no rest step was included in the cycling protocol, then the coulombic efficiency was 73%. However, the coulombic efficiency was only 23% after a rest of 72 hours. This experiment indicates that lithiated MIL-101(Fe) suffers from an irreversible relaxation mechanism that reduces reversibility.

Like many battery materials, MOFs tend to undergo a conversion reaction if lithiated beyond a certain point. Very often this conversion reaction is irreversible. In the case of MOFs, if Fe^{3+} is reduced beyond a certain point, this results in the disintegration of the material structure.[13,25] Synchrotron PXRD was utilized in order to determine if any significant structural changes occur during cycling which could account for MIL-101(Fe)'s poor reversibility (Fig. 3). A simulated PXRD pattern of MIL-101(Cr) was utilized as a reference.[26] MIL-101(Fe) shows some minor secondary phase peaks that are related to irreversible SP decomposition in the electrochemical cell. In addition, a reversible change in intensity was observed for some peaks including the (022) peak. These changes in intensity are attributed to solvent molecules intercalating along with the Li^+. Further discussions regarding the secondary phases and the intensity changes are described in the ESI.† Most importantly, the irreversible changes in the diffraction patterns were only related to the secondary phase, suggesting that MIL-101(Fe) was stable during cycling and that the poor capacity retention was not due to disintegration of the framework.

In operando XAS of the Fe K-edge was used to characterize the short range structural changes occurring in MIL-101(Fe) during a full lithiation/de-lithiation cycle at a rate of C/20. In the XAS experiment, MIL-101(Fe) only achieved an initial discharge capacity of 0.3 Li/Fe, whereas in the C/20 experiment without the beam (Fig. 2c), MIL-101(Fe) could achieve an initial discharge capacity of 0.57 Li/Fe at the same rate. We suspect

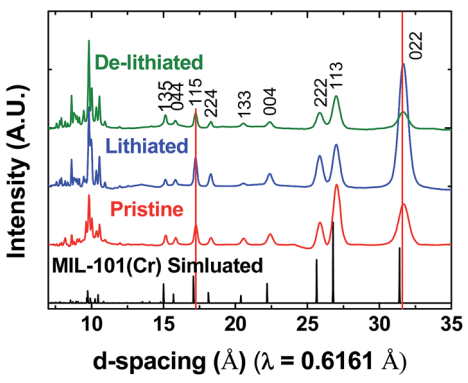

Fig. 3 Synchrotron PXRD patterns for MIL-101(Fe) prior to cycling (red), after lithiation (blue), and after de-lithiation (green). Patterns are compared to a simulated pattern of the MIL-101(Cr) analogue structure. Red lines indicate peaks that show a reversible change in intensity.

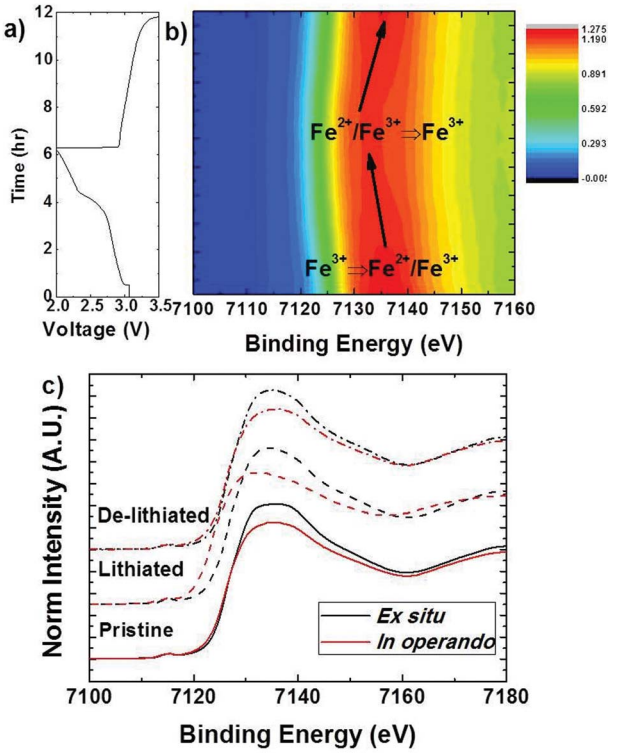

Fig. 4 *In operando* and *ex situ* XANES of MIL-101(Fe). (a) Voltage profile with respect to the *in operando* XAS scanning time. (b) The contour plot of the *in operando* XAS XANES region *versus* time indicates a reversible change in the Fe oxidation state. (c) Comparison of the *in operando* (red) and *ex situ* (black) XAS XANES spectra. The Fe K-edge of the *ex situ* lithiated sample does not shift to a lower binding energy that indicates the presence of a time dependent fade mechanism.

that irradiation of the sample during the *in operando* XAS measurement contributed to a lower lithium insertion capacity.[27,28] Fig. 4a presents a contour plot of the XANES region with respect to measurement time where it is observed that the Fe K-edge shifts to lower binding energy during lithiation and then reversibly shifts back to its pristine binding energy upon de-lithiation. A shift to a lower binding energy during lithiation is consistent with the reduction of Fe^{3+} to a mixed valence state of Fe^{3+} and Fe^{2+}. Upon de-lithiation, the mixed valence state is oxidized back to Fe^{3+}. Because the binding energy shift is reversible, *in operando* XAS also does not explain the poor capacity retention of MIL-101(Fe) (Fig. 2d).

Unlike the *in operando* XAS or PXRD experiments, the results of our *ex situ* XAS experiment help describe the time dependent capacity fade mechanism. Fig. 4b presents a comparison between the *in operando* and *ex situ* XANES spectra of MIL-101(Fe) in its pristine, lithiated, and de-lithiated states. The time between electrode preparation and *ex situ* XAS measurement was 3–4 days. Our first observation was that the spectra intensities near the Fe K-edge were always lower for the *in operando* samples. This can be explained by the fact that the *in operando* samples were thicker than the *ex situ* samples such that more signal was lost to self absorption.[29,30] More importantly, the K-edge of the lithiated *ex situ* sample did not shift to a lower binding energy as it did for the lithiated *in operando* sample. This result indicates that the Fe^{3+}/Fe^{2+} mixed valence state formed upon lithiation is not stable over longer times. For this reason, the Fe^{3+}/Fe^{2+} mixed valence state can be observed only using *in operando* XAS.

A contour plot of the *in operando* XAS experiment Fourier transformed EXAFS spectra is provided in Fig. 5. The Fourier transform of the EXAFS region is correlated with the radial distribution of nearest neighbor atoms about Fe. The nearest neighbor atoms for Fe are observed at approximately 1.5 Å. In the pristine state, the three Fe ions of the SBU are coordinated with 17 O and one Cl nearest neighbor. The intensity of the spectrum at 1.5 Å decreases upon lithiation and then increases again upon de-lithiation. We attribute the variability of intensity to a reversible change in the coordination environment of the nearest neighbors. Cl^- ions are known to be labile[31] and scatter X-rays more intensely than O^{2-} ions. With this in mind, it may be possible that for each Fe, one O atom from an electrolyte solvent molecule replaces Cl^- ion upon full lithiation.

To gain further insight into the EXAFS results, electronic structure calculations on the MIL-101(Fe) SBU were performed. A simplified SBU model (Trimer, Fig. S2a†) was used in the calculations. Similarly to the model provided in Fig. 1a, the SBU model includes the three Fe centers, but replaces the benzene groups with methyl groups in order to reduce the computational cost. An additional model (TrimerDMC, Fig. S2b†) has also been investigated. In this second model, the axial Cl has been replaced by a carboxylate group, coordinated to the Fe center *via* one oxygen atom from the carbonyl group. Both models have been used to evaluate the changes in the free energy associated with incremental reduction of the metal centers.

Because there are different reduction centers in the two models, all possible combinations were calculated (Fig. 6 and Table S2†). In Fig. 6, blue and green dots are used to simply represent the electronic structure of Fe. The calculated free energy of the reduced SBUs was found to be largely independent of the particular Fe center reduced. The first electron reduction of Fe (one green dot, one Fe center reduction Fe^{3+}/Fe^{2+}) required −3.13 eV for the Trimer model and −6.46 eV for the TrimerDMC model. In all four cases one electron reduction is associated with a negative ΔG indicating that both models strongly prefer

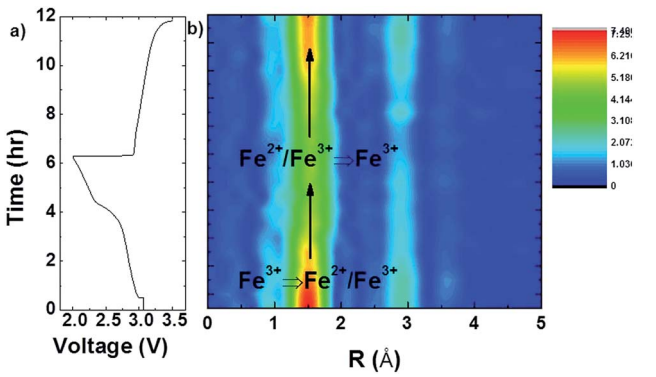

Fig. 5 Fourier transformed EXAFS region of the *in operando* XAS data. (a) Voltage profile with respect to the *in operando* XAS scanning time. (b) Contour plot of the EXAFS region *versus* time that indicates a reversible change in Fe coordination during cycling.

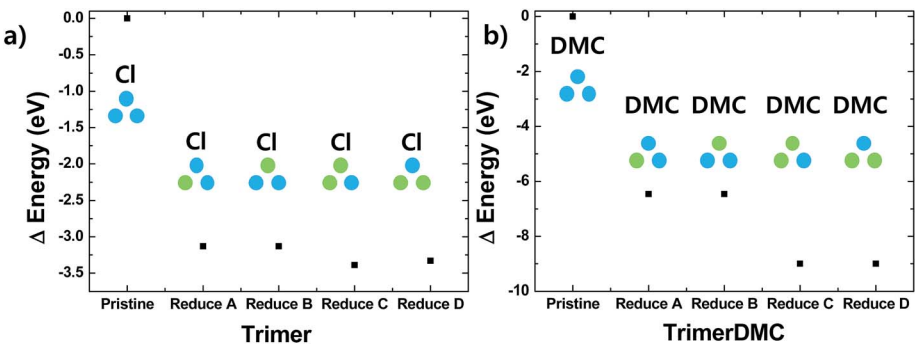

Fig. 6 Gibbs free energies relative to the respective pristine state are shown for the (a) Trimer and (b) TrimerDMC models and their reduced forms. Insets: oxidation states of Fe for the respective reduced states are illustrated in simple dots. Blue dots are Fe^{3+} and green dots are Fe^{2+}.

to exist in a reduced state. These results indicate that the reduction of the MIL-101(Fe) SBU is twice as favorable when a DMC molecule is coordinated to the iron metal center, and that Cl^- coordination can slow down the reduction process. Furthermore, the second electron reduction (2 green dots, two Fe center reductions Fe^{3+}/Fe^{2+}) requires −3.36 eV for the Trimer model and −9.00 eV for the TrimerDMC model. In both cases, addition of a second electron provides with further stabilization on the system. However, the reduced TrimerDMC model is much more stable than the Trimer model. This allows us to conclude that substituting Cl^- for a DMC molecule makes the MIL-101(Fe) MOF much more prone to a two electron reduction, results that can be correlated with the changes in the PXRD peak intensities with cycling (Fig. 3).

Discussion

Relaxation of Fe^{2+} to Fe^{3+} will result in the irreversible accumulation of Li^+ ions in MIL-101(Fe). As more Li^+ ions accumulate, MIL-101(Fe) loses potential Li^+ ion insertion sites and empty Li^+ site energy drastically increases for future cycles. Computational work on MIL-53(Fe) supports this notion.[25] As the sites fill up, the energy required for additional Li^+ insertion will eventually surpass the free energy of Fe^{3+} reduction. It is the constant accumulation of Li^+ ions that cause the capacity of MIL-101(Fe) to rapidly fade.

In addition to the *in operando* EXAFS, we conducted an *ex situ* EXAFS experiment (Fig. S3 and S4†). *Ex situ* EXAFS spectra were collected after the MIL-101(Fe) MOF electrode was reduced to 2.5 V and again after the electrode was further reduced to 2.0 V. Although the first neighbor peak intensity was identical for the pristine and the 2.5 V sample, there is a reduction in the first neighbor peak intensity for the 2.0 V sample. When the electrode was oxidized back to 3.5 V, the first neighbor peak did not completely regain intensity. The *ex situ* EXAFS data thus provide further support for our computational results suggesting that Cl^- ions may be irreversibly replaced by DMC molecules in order to decrease the free energy of Fe site reduction.

A major point provided from the electronic structure calculations is the significant difference observed in the free energy profiles associated with the changes in the axial coordination sphere of the iron metal center. Different coordination spheres lead to different behaviors towards reduction, thus affecting the recycling efficiency of the material, because a Cl^- ion can be more easily detached from the coordination sphere. As observed in Fig. 2d, a longer rest time between the lithiation and de-lithiation reduces the coulombic efficiency. This temporal effect can be associated with Cl^- ligand lability. After lithiation, the Cl^- ligand can dissociate from the Fe center, and with longer times, the anion can diffuse further away from the metal center. This may have detrimental effects on the electrochemical performance since MIL-101(Fe) will not regain its pristine structure after de-lithiation. One way to try to avoid such irreversible change is to switch Cl^- to F^- to strengthen the bond between Fe and F. However, this will require the use of HF. Other possible ways to improve the reversibility of the MIL-101(Fe) redox would be to improve the stability of its reduced SBU. To stabilize the SBU, one can alter the electronic structure of the SBU. Many studies have demonstrated different pathways to alter the electronic structure *via* ligand functionalization,[35] by increasing the conjugation on the system.[9] In addition, one can replace the ligands with other redox active organic molecules such as benzoquinones,[32] organic radicals,[8,33,34] or oxocarbons.[35]

Conclusions

In this work, the MIL-101(Fe) MOF was tested as an electrode for use in lithium ion batteries. The redox chemistry (Fe^{2+}/Fe^{3+}) was found to not be completely reversible. We characterized the decay mechanism using *ex situ* and *in operando* XAS measurements. The Fe^{2+} oxidation state was not observed from *ex situ* experiments. The temporal dependency of Fe^{2+} observation indicates the importance of *in operando* experiments. The computational results indicate that significant energy differences can be expected between the pristine and reduced forms of MIL-101(Fe). This is ascribed to the axial ligand coordinated to the Fe^{3+} metal centers. Our study thus suggests that an appropriate functionalization of the MIL-101(Fe) SBUs can improve the reversibility of the Fe^{2+}/Fe^{3+} redox reaction.

Acknowledgements

This work is supported by the University of California, San Diego's Chancellor's Interdisciplinary Collaboratories Award. Use of the Advanced Photon Source, an Office of Science User Facility operated for the U.S. Department of Energy (DOE) Office of Science by Argonne National Laboratory, was supported by the U.S. DOE under Contract no. DE-AC02-06CH11357. The theoretical and computational analyses were supported by the National Science Foundation (Award Number DMR-1305101 to F.P.) and used resources of the Extreme Science and Engineering Discovery Environment (XSEDE), which is supported by the National Science Foundation Grant Number OCI-1053575 (Allocation TG-CHE110009 to F.P.). MOF synthesis was also supported by a grant from the Department of Energy, Office of Basic Energy Sciences, Division of Materials Science and Engineering under Award no. DE-FG02-08ER46519 (S.M.C.). The authors would also like to thank Prof Eric Fullerton at UCSD for the access to magnetic susceptibility measurements.

References

1 M. Armand and J. M. Tarascon, *Nature*, 2008, **451**, 652–657.
2 F. S. Anthony, *J. Chem. Educ.*, 1983, **60**, 320.
3 J. Tarascon and M. Armand, *Nature*, 2001, **414**, 359–367.
4 J.-M. Tarascon, *ChemSusChem*, 2008, **1**, 777–779.
5 J. M. Pearce, *Int. J. Nucl. Governance, Econ. Ecol.*, 2008, **2**, 17.
6 W. Walker, S. Grugeon, O. Mentre, S. Laruelle, J. M. Tarascon and F. Wudl, *J. Am. Chem. Soc.*, 2010, **132**, 6517–6523.
7 W. Walker, S. Grugeon, H. Vezin, S. Laruelle, M. Armand, J. M. Tarascon and F. Wudl, *Electrochem. Commun.*, 2010, **12**, 1348–1351.

8 K. Nakahara, S. Iwasa, M. Satoh, Y. Morioka, J. Iriyama, M. Suguro and E. Hasegawa, *Chem. Phys. Lett.*, 2002, **359**, 351–354.
9 S. E. Burkhardt, J. Bois, J. M. Tarascon, R. G. Hennig and H. D. Abruna, *Chem. Mater.*, 2013, **25**, 132–141.
10 J. Kim, B. L. Chen, T. M. Reineke, H. L. Li, M. Eddaoudi, D. B. Moler, M. O'Keeffe and O. M. Yaghi, *J. Am. Chem. Soc.*, 2001, **123**, 8239–8247.
11 C. Mellot-Draznieks, J. Dutour and G. Férey, *Z. Anorg. Allg. Chem.*, 2004, **630**, 2599–2604.
12 L. Xiaoxia, C. Fangyi, Z. Shuna and C. Jun, *J. Power Sources*, 2006, **160**, 542–547.
13 G. Férey, F. Millange, M. Morcrette, C. Serre, M.-L. Doublet, J.-M. Grenèche and J.-M. Tarascon, *Angew. Chem., Int. Ed. Engl.*, 2007, **46**, 3259–3263.
14 F. Alexandra, H. Patricia, D. Thomas, S. Christian, M. Jérôme, G. Jean-Marc, M. Mathieu, T. Jean-Marie, M. Guillaume and F. Gérard, *Eur. J. Inorg. Chem.*, 2010, **2010**, 3789–3794.
15 J. Overgaard, F. K. Larsen, B. Schiott and B. B. Iversen, *J. Am. Chem. Soc.*, 2003, **125**, 11088–11099.
16 A. K. Dutta, S. K. Maji and S. Dutta, *J. Mol. Struct.*, 2012, **1027**, 87–91.
17 A. K. Boudalis, Y. Sanakis, F. Dahan, M. Hendrich and J. P. Tuchagues, *Inorg. Chem.*, 2006, **45**, 443–453.
18 K. Taylor-Pashow, J. Della Rocca, Z. Xie, S. Tran and W. Lin, *J. Am. Chem. Soc.*, 2009, **131**, 14261–14263.
19 G. Férey, F. Millange, M. Morcrette, C. Serre, M. L. Doublet, J. M. Greneche and J. M. Tarascon, *Angew. Chem., Int. Ed.*, 2007, **46**, 3259–3263.
20 A. P. Hammersley, ESRF Internal Report, 1997, ESRF97HA02T.
21 A. P. Hammersley, S. O. Svensson, M. Hanfland, A. N. Fitch and D. Häusermann, *High Pressure Res.*, 1996, **14**, 235–248.
22 B. Ravel and M. Newville, *J. Synchrotron Radiat.*, 2005, **12**, 537–541.
23 A. D. Becke, *J. Chem. Phys.*, 1993, **98**, 5648–5652.
24 A. Schafer, C. Huber and R. Ahlrichs, *J. Chem. Phys.*, 1994, **100**, 5829–5835.
25 C. Combelles, M. Ben Yahia, L. Pedesseau and M. L. Doublet, *J. Phys. Chem. C*, 2010, **114**, 9518–9527.
26 G. Férey, C. Mellot-Draznieks, C. Serre, F. Millange, J. Dutour, S. Surble and I. Margiolaki, *Science*, 2005, **309**, 2040–2042.
27 S. V. Antonyuk and M. A. Hough, *Biochim. Biophys. Acta, Proteins Proteomics*, 2011, **1814**, 778–784.
28 J. Qiu, L. Cao, P. Mulligan, D. Turkoglu, S. C. Nagpure, M. Canova and A. Co, *IEEE Trans. Nucl. Sci.*, 2013, **60**, 662–667.
29 E. A. Stern and K. Kim, *Phys. Rev. B: Condens. Matter Mater. Phys.*, 1981, **23**, 3781–3787.
30 C. H. Booth and F. Bridges, *Phys. Scr., T*, 2005, **115**, 202.
31 Y. P. Ou, D. Feng and J. J. Yuan, *Acta Crystallogr., Sect. E: Struct. Rep. Online*, 2010, **66**, M921–U558.
32 T. Le Gall, K. H. Reiman, M. C. Grossel and J. R. Owen, *J. Power Sources*, 2003, **119**, 316–320.
33 J. Q. Qu, T. Katsumata, M. Satoh, J. Wada and T. Masuda, *Macromolecules*, 2007, **40**, 3136–3144.
34 H. Nishide, S. Iwasa, Y. J. Pu, T. Suga, K. Nakahara and M. Satoh, *Electrochim. Acta*, 2004, **50**, 827–831.
35 H. Chen, M. Armand, G. Demailly, F. Dolhem, P. Poizot and J. M. Tarascon, *ChemSusChem*, 2008, **1**, 348–355.

